THE ASTROPHYSICAL JOURNAL, 279:60–73, 1984 April 1

3C 111: A LUMINOUS RADIO GALAXY WITH A HIGHLY COLLIMATED JET

ROGER LINFIELD
University of California, Radio Astronomy Laboratory

AND

RICK PERLEY
National Radio Astronomy Observatory
Received 1983 May 31; accepted 1983 September 16

ABSTRACT

The luminous radio galaxy 3C 111 has been mapped at 20, 6, and 2 cm with the VLA. A one-sided, highly collimated jet is seen, emerging from the core in PA 63°, and eventually leading into the hot spot at the leading edge of the NE lobe, 120″ from the core. There is probably an active but undetected counterjet feeding the SW lobe. The main jet appears to be neither free nor thermally confined; magnetic self-confinement is suggested. A set of six nearly periodic knots in the jet may be due to the periodic oblique shocks predicted by numerical simulations.

Subject headings: galaxies: individual — galaxies: jets — radio sources: galaxies

I. INTRODUCTION

The necessity of a continuous or quasi-continuous energy supply to the outer lobes of extended radio sources has been well established (Hargrave and Ryle 1974; Longair, Ryle, and Scheuer 1973). With recent observations it has become increasingly certain that this supply takes the form of jets originating in the core of the associated quasar or galaxy. In the majority of low luminosity ($L_{1.4} < 10^{25}$ W Hz^{-1}) sources ($L_{1.4}$ is the luminosity at 1.4 GHz), these jets are visible on scales from parsecs to kiloparsecs (e.g., in NGC 6251, Readhead, Cohen, and Blandford 1978; Perley, Bridle, and Willis 1984; NGC 315, Linfield 1981 and Willis *et al.* 1981).

However, the relationship between the observed jets and the underlying energy transport is vague at best, and the physics of this transport is very uncertain. In higher luminosity ($L_{1.4} > 10^{25}$ W Hz^{-1}) sources, where powerful beams are expected, jets are normally absent, or, if present, are seen only in the inner few parsecs, with a large gap between them and the outer lobes. Jet surface brightness is not proportional to source luminosity. The available data are consistent with a surface brightness independent of source luminosity. However, this conclusion is still uncertain because the dynamic range required to detect a jet of a given surface brightness increases with source luminosity. Recent very high dynamic range observations of Cyg A have revealed a kiloparsec-scale jet (R. Perley 1983, private communications).

Actual detection of kiloparsec-scale jets in high-luminosity extended sources would help resolve the issue. Toward that end, observations of the luminous ($L_{1.4} = 6.8 \times 10^{25}$ W Hz^{-1}) radio galaxy 3C 111 were made with the Very Large Array. 3C 111 exhibits the Fanaroff and Riley (1974) type II morphology. It has a bright core, which displays a prominent, one-sided jet on a milli-arcsecond scale (Linfield 1981). The observations are described in the following section. The maps are presented in § III. In § IV the physical properties of the jet, including the questions of jet confinement and stability, are discussed. Some conclusions are given in § V.

II. OBSERVATIONS

This source was observed in 1982 June, at 1.4, 4.9, and 15 GHz with the VLA in the A configuration. Details of the VLA are given by Thompson *et al.* (1980). Observing times, bandwidths, and resulting beamwidths are given in Table 1. At 1.4 and 4.9 GHz the entire source was mapped in one field, with the central component at the phase tracking center. At 15.0 GHz, the SW lobe was too weak and extended to detect, so the phase tracking center was moved 20″ from the core in the direction of the NE lobe. This allowed the core and the NE lobe to be mapped in one primary antenna beam.

Calibrator sources (3C 84 and 3C 138) were observed approximately once every 90 minutes, at each frequency. These observations were used to solve for instrumental phase and polarization. 3C 286 was observed to establish the flux density scale; fluxes of 14.6, 7.4, and 3.44 Jy at the three frequencies were assumed (Baars *et al.* 1977). The data were then gridded, fast Fourier transformed, and cleaned using the method of Clark (1980). An antenna-based self-calibration scheme (Schwab 1980) was then used to improve the dynamic range of the maps. This technique is very effective for a source such as 3C 111 which has a strong compact component; the dynamic ranges of the 4.9 and 15.0 GHz maps are limited primarily by their thermal noise levels, at dynamic ranges of 2000:1 and 1200:1, respectively. The dynamic range of the 1.4 GHz map (1000:1) is limited by systematics, as the core is less dominant than at higher frequencies. At 4.9 GHz the dynamic range was increased by including some data obtained by J. Dreher at an earlier epoch.

III. RESULTS

a) *Jet*

The 1.4 GHz total intensity map is shown in Figure 1. A highly collimated jet is visible, leading from the core to the NE lobe. The dynamic range is barely adequate to detect the jet, and except in the inner 20″ it is only visible intermittently.

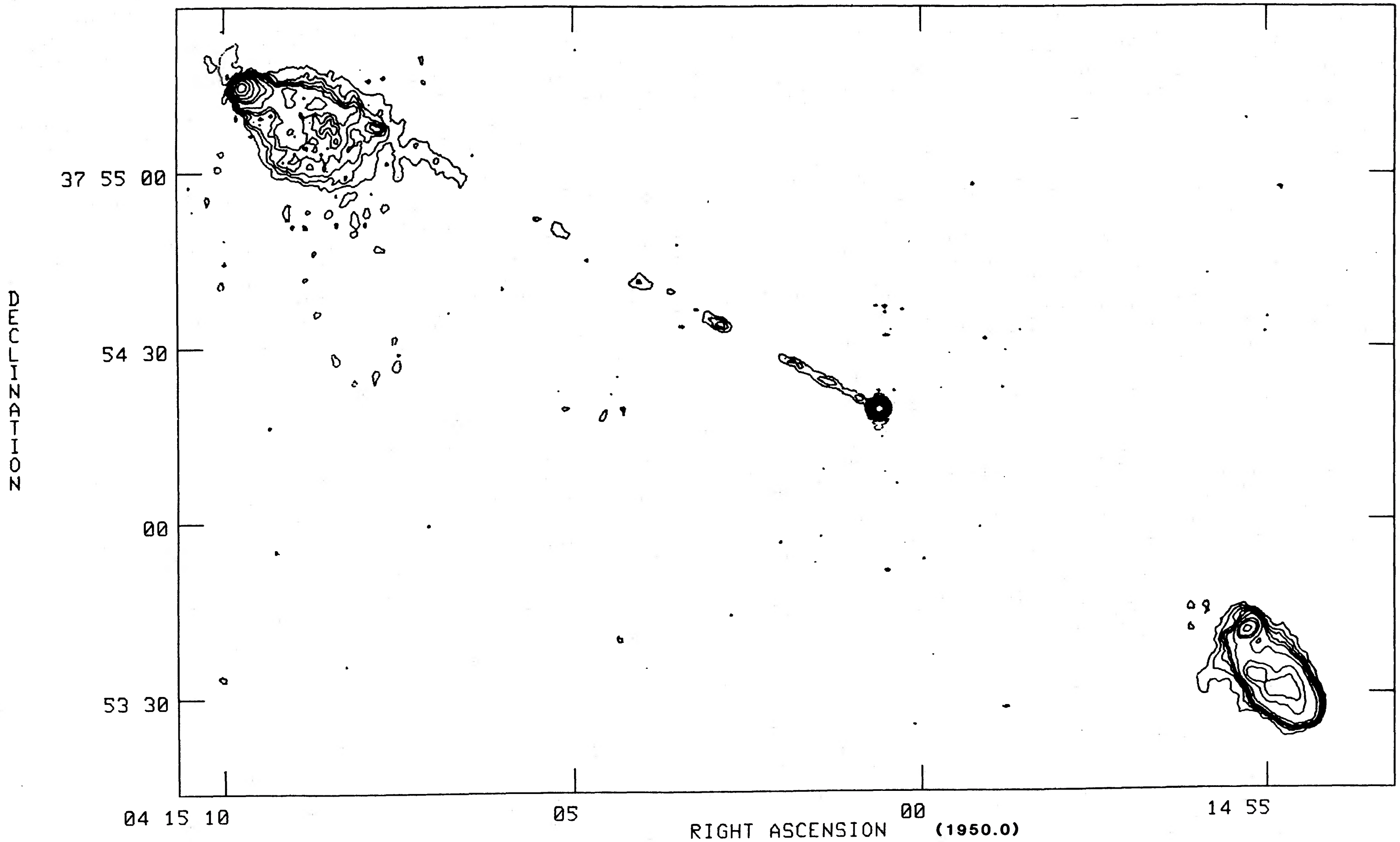

FIG. 1.—Total intensity map of 3C 111 at 1.4 GHz, with 1.″34 × 1.″20 resolution. The bright central component is coincident with the nucleus of the optical galaxy. The contour levels are −3.7, −1.2, 1.2, 2.5, 3.7, 4.9, 6.1, 9.8, 22, 37, 86, 220, and 470 mJy per beam.

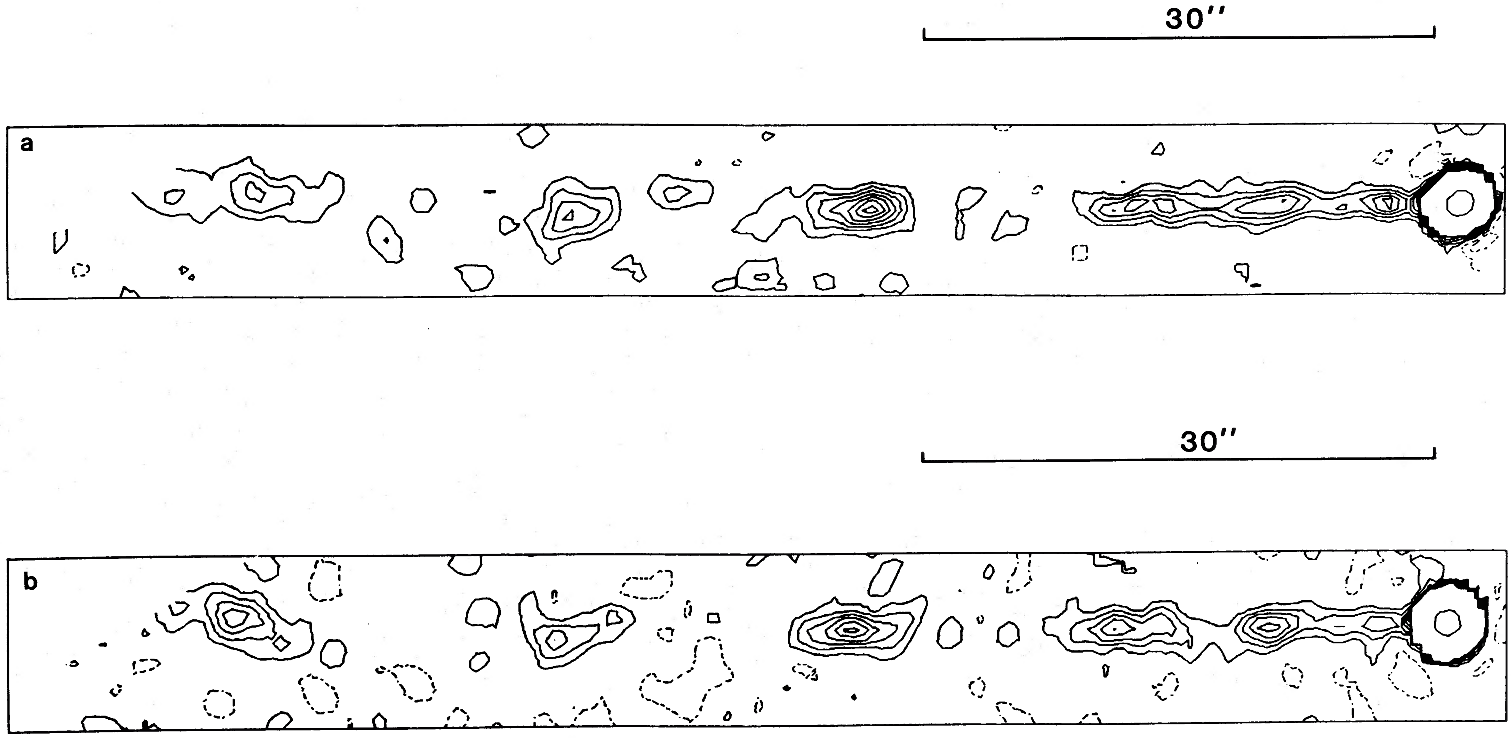

FIG. 2.—Total intensity maps of the inner 65″ of the 3C 111 jet, rotated through 29°. (*a*) 1.4 GHz map, with 1″.34 × 1″.20 resolution. The contour levels are −1.89, −0.63, 0.63, 1.26, 1.89, 2.52, 3.1, 3.8, 4.4, and 450 mJy per beam. (*b*) 4.9 GHz map, with 1″.31 × 1″.24 resolution. The contour levels are −0.94, −0.31, 0.31, 0.63, 0.94, 1.25, 1.56, 1.88, and 520 mJy per beam.

TABLE 1

OBSERVING PARAMETERS

Observing Frequency (GHz)	Observing Time (minutes)	Bandwidth (MHz)	Synthesized Beam
1.4	140	6.25	1".34 × 1".20 −88°
4.9	147	12.5	0".40 × 0".36 −88°
15.0	295	25.0	0".13 × 0".12 −88°

The jet merges into the NE lobe along the northern border of the lobe. It then curves sharply, and terminates in the hot spot at the leading edge of the lobe. In Figure 1 the jet is difficult to trace once it enters the lobe. This part of the jet is more prominent at 4.9 GHz (Fig. 6*b*); it has a flatter spectral index than does the remainder of the lobe. In Figure 6*b* the jet can be traced to within 4" of the lobe hot spot but can be seen only intermittently (as is the case nearer the core).

No counterjet is visible, but due to the limited dynamic range this does not demand a large jet:counterjet flux ratio. A similar counterjet would be visible if its intensity were less than 20% of the intensity of the observed jet. If the counterjet had a uniform intensity (i.e., no knots), the upper limit would be 35% of the jet intensity.

Figure 2 shows the inner 65" of the jet in more detail, at 1.4 GHz (Fig. 2*a*) and at 4.9 GHz (Fig. 2*b*). The 4.9 GHz map was made with the data tapered to give a resolution similar to that of the full resolution 1.4 GHz map (Fig. 2*a*). The jet has a nonuniform brightness distribution; the emission is concentrated in a few knots (six knots are visible in Fig. 2). Except in the inner 20" no emission was detected between the knots; the knot 30" from the core has a contrast >6 with its surroundings.

Figure 3 shows the region near the core at 4.9 GHz. Here only the inner 1".5 are definitely detected, although several knots (9", 17", and 30" from the core) outside the field of Figure 3 were detected. The core is too strong to allow detection of the jet closer than 0".7. In polarized intensity, where the core is much weaker, the jet can be seen as close to the core as 0".4. At 15.0 GHz the jet was not detected: this implies that the jet emission per unit length falls off less rapidly than $\Theta^{-1.1}$ from $\Theta = 0''.25$ to $1''.00$ (using the spectral index of 0.6 measured between 1.4 and 4.9 GHz). (Θ is the distance from the core.)

Figure 4 shows the variation of jet position angle (PA) with distance from the core. Except at $\Theta = 0''$ and $\Theta > 90''$, values are plotted on Figure 4 only for locations where emission is seen at both 1.4 GHz and 4.9 GHz (with the data tapered to give a resolution similar to that at 1.4 GHz). The plotted values are the averages of the position angles at the two frequencies, and the error bars represent estimated 2 σ errors. The datum at $\Theta = 0''$ was taken from VLBI observations at 10.7 GHz (Linfield 1981). At $\Theta > 90''$ (i.e., inside the NE lobe) the contrast between the jet and its surroundings is low at 1.4 GHz, and the plotted data are from measurements at 4.9 GHz only. The value at $\Theta = 121''.5$ corresponds to the hot spot in the NE lobe (visible at both frequencies).

The jet is remarkably straight for the first 60", with no detectable curvature. From $\Theta = 60''$ to $\Theta = 65''$ its position angle changes from $61^\circ.4 \pm 0^\circ.3$ to $60^\circ.2 \pm 0^\circ.2$. The jet is straight from $\Theta = 65''$ to $\Theta = 104''$ (inside the NE lobe). Beyond

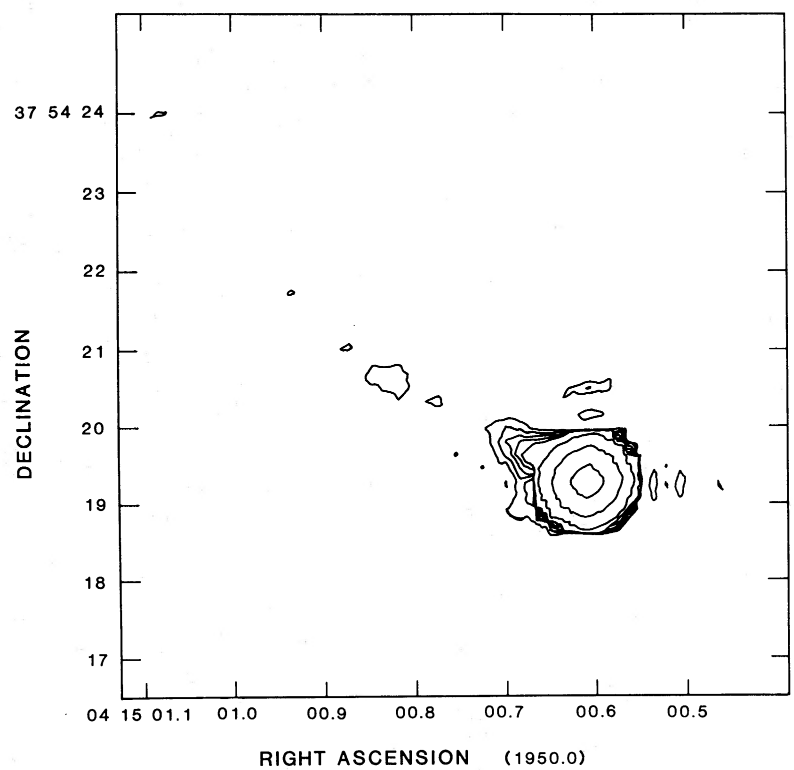

FIG. 3.—Inner region of the jet at 4.9 GHz, with 0".40 × 0".36 resolution. Contour levels are −1.03, −0.34, 0.34, 0.68, 1.03, 1.37, 1.71, 6.2, 68, and 570 mJy per beam.

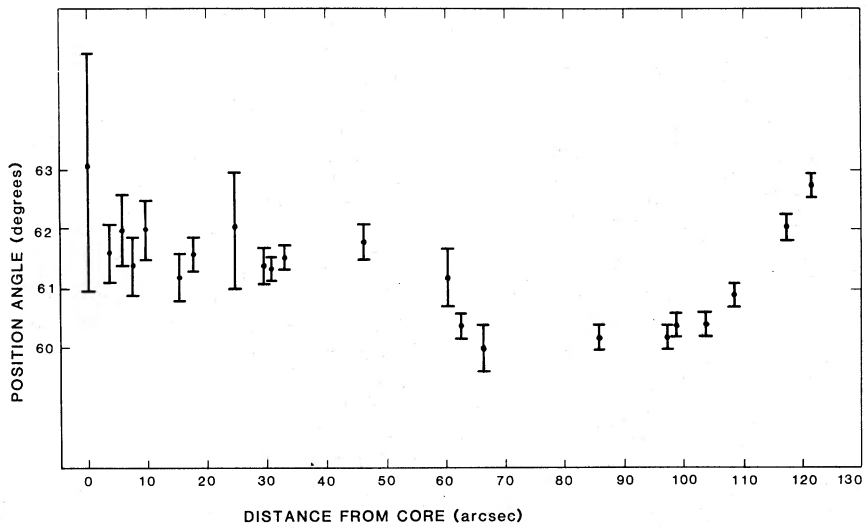

FIG. 4.—Jet position angle (PA) vs. distance (Θ) from the core. The vertical bars represent estimated 2 σ errors. The datum at $\Theta = 0''$ is taken from VLBI observations. The datum at $\Theta = 121''$ is of the hot spot in the NE lobe

$\Theta = 104''$ the jet bends sharply and terminates at the lobe hot spot, at PA $62\overset{\circ}{.}74 \pm 0\overset{\circ}{.}2$.

The variation of jet width Ω is shown in Figure 5. One-dimensional Gaussians were fitted to profiles of the jet "core" (defined as that part of the jet with intensity >0.5 mJy per beam at 1.4 GHz, >0.2 mJy per beam at 4.9 GHz). The resultant widths (FWHM) were deconvolved from the effects of the restoring beam, to give a net width. The values plotted in Figure 5 are the averages of the net widths at the two frequencies (1.4 GHz and 4.9 GHz, with comparable resolutions). The error bars represent estimated 2 σ errors. There are no systematic differences in the jet widths at the two frequencies.

With the constraint that the jet width is 0 at the core, it can be concluded that the jet expands rapidly in the inner 20″, followed by a more gradual expansion. Beyond 40″, the width appears to increase slowly, if at all.

The spectral index of the jet, as measured from maps at 1.4 and 4.9 GHz, averages 0.6 ($S \propto \nu^{-\alpha}$), where the jet is visible. The jet is too weak to allow the determination of spectral index variations over this narrow a frequency range.

At 1.4 GHz no polarized emission was detected from the jet. This yields weak upper limits on the jet polarization at this frequency. The brightest knot, 31″ from the core, is less than 20% polarized at the location of its total intensity peak. Other bright knots are less than 30% polarized at their total intensity

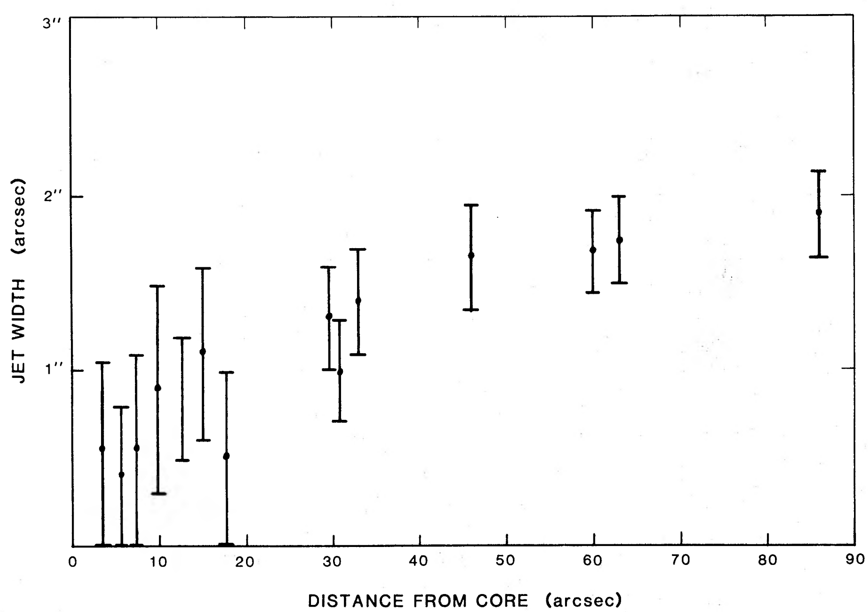

FIG. 5.—Jet width (Ω) vs. distance (Θ) from the core. The width plotted is the FWHM, deconvolved from the restoring beam.

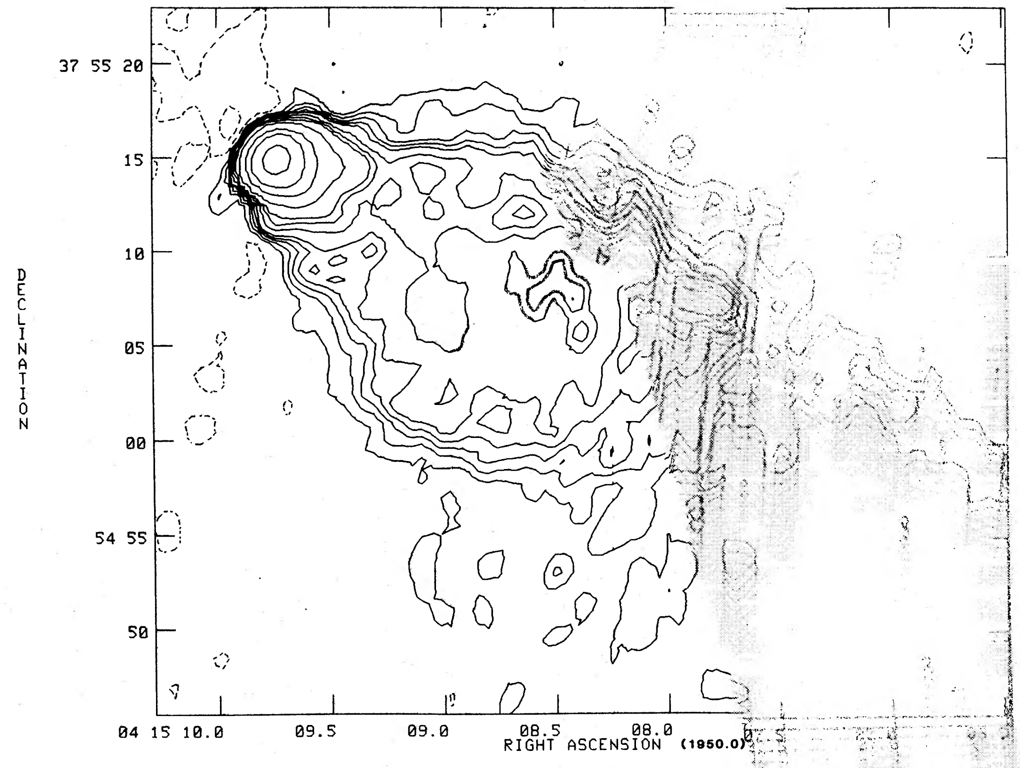

FIG. 6a

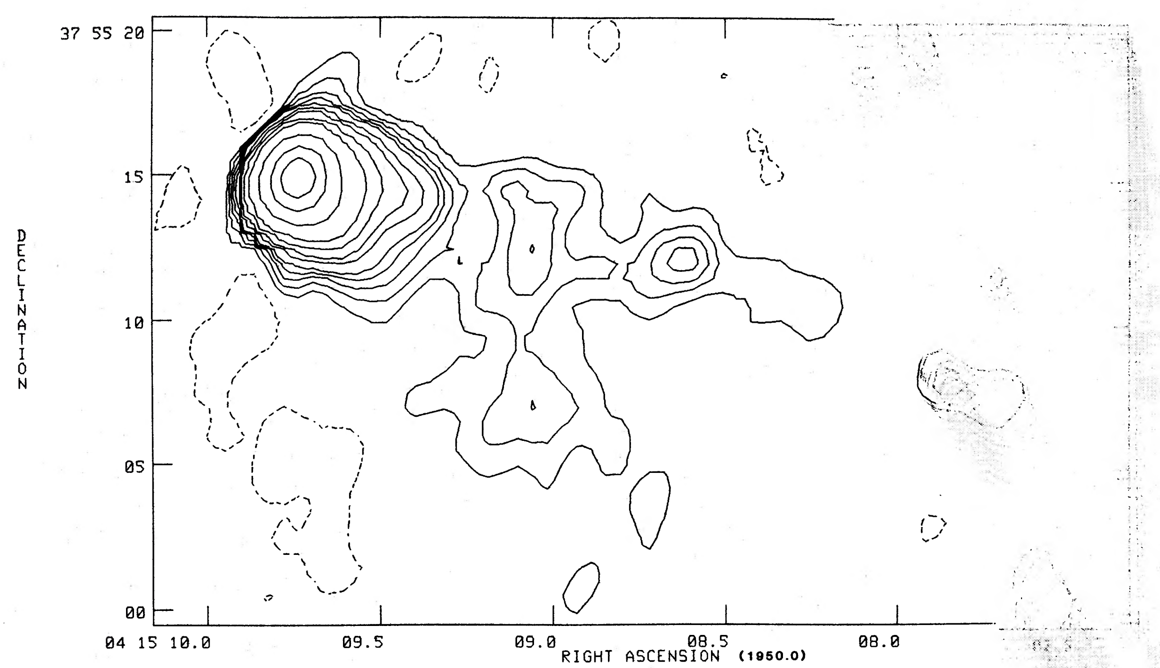

FIG. 6b

FIG. 6.—Total intensity maps of the NE lobe of 3C 111. (*a*) At 1.4 GHz, with 1″34 × 1″20 resolution. The contour levels are 3.8, 4.7, 7.6, 10.4, 13, 28, 76, 170, and 470 mJy per beam. (*b*) At 4.9 GHz, with 1″31 × 1″24 resolution. The contour levels are −2.3, 3.8, 6.2, 8.5, 13.9, 23, 62, 140, and 230 mJy per beam.

TABLE 2

CORE PARAMETERS

Frequency (GHz)	Core Flux (Jy)	Fractional Polarization (percent)
1.4	0.95	0.80
4.9	1.14	0.95
15.0	1.24	1.3

peaks. The emission between knots in the inner 15″ is less than 50% polarized.

At 4.9 GHz, polarized emission is seen in the inner 1″.3 of the jet. The fractional polarization is ~30%. With a polarization map at only one frequency, the magnetic field orientation cannot be determined. The values of the core flux and the fractional polarization of the core at the three frequencies are given in Table 2.

b) *Lobes*

Figure 6 shows the NE lobe at 1.4 and 4.9 GHz, with ~1″.3 resolution. This lobe fits well into the type II classification of Fanaroff and Riley (1974) in having a compact hot spot at a sharp leading edge. A low surface brightness tail stretches back towards the core. The tail has a full opening angle of 65°, and a length of ~25″; outside this cone, and beyond this distance its brightness drops rapidly (except along the jet).

The two point spectral index of the lobe $\alpha_{4.9}^{1.4}$ is 0.7 at the hot spot and steepens toward the core. At 7″ from the hot spot, $\alpha_{4.9}^{1.4} = 1.4$. The knots 8″, 14″, and 23″ from the hot spot have spectral indices at their peaks of 1.05, 1.15, and 1.1, respectively (the uncertainty is 0.1 in each of these values); the intervening regions have $\alpha > 1.5$. The jet has a much flatter spectral index than does the surrounding region of the lobe.

The hot spot at the leading edge of the lobe is shown at a resolution of ~0″.3 in Figure 7, at 4.9 GHz and 15.0 GHz. The 15.0 GHz map was made with strongly tapered data; there is no evidence for structure <0″.3 in size in this lobe. The hot spot displays the blunt leading edge seen in other similar sources (Dreher 1981); the HWHM of the leading edge is 0″.33.

The polarization of the NE lobe is shown in Figure 8. Most of the interior of the lobe is <10% polarized at 1.4 GHz. The region 1″–5″ behind the hot spot is ~15% polarized. Along the SE edge of the lobe the percentage polarization ranges from 20% to 35%; along the N edge it ranges up to 45%. The projected magnetic field appears to be parallel to the edges of the lobe, in the hot spot (Fig. 8*b*) and in the more diffuse regions of the lobe (Fig. 8*a*). This conclusion is uncertain, due to the lack of sufficient frequency coverage to determine the rotation measure. The integrated rotation measure for 3C 111 is only -19 rad m^{-2} (Simard-Normandin, Kronberg, and Button 1981), so the RM is likely to be small throughout the source. For the hot spot, *E*-vector PAs at 1.4 and 4.9 GHz agree everywhere to within a few degrees; the projected magnetic field in the hot spot is therefore probably nearly perpendicular to the vectors plotted in Figure 8*b*. The fractional polarization of the hot spot at 1.4 GHz is 0.85 that at 4.9 GHz.

The SW lobe is shown in Figure 9. As the spectral index gradients in this lobe are small, only the 1.4 GHz map is presented. There is a hot spot near the trailing edge; it is elongated perpendicular to the source axis, with dimensions (FWHM) 2″.1 × 1″.1. A more diffuse structure extends ~20″ to the SW. It has a plateau of roughly constant surface brightness; the edge of this plateau is separated from the hot spot by ~5″. There is also some very diffuse emission extending from the hot spot back toward the core, but it is too weak and too diffuse to be adequately mapped with the present data set.

The polarization of the SW lobe is shown in Figure 10, at 4.9 GHz. The axis of the lobe is ~15% polarized; the percentage of polarization increases to ~45% at the edges of the lobe. At 1.4 GHz, with the same resolution, the percentage of polarization is 0.80 that at 4.9 GHz. The polarization angles at 1.4 and 4.9 GHz differ by ~20°, except near the center of the "plateau," where the difference is ~40° in the same direction. The projected magnetic field is therefore probably nearly perpendicular to the vectors in Figure 10. The projected field is approximately circumferential, both in the hot spot, and in the lobe as a whole.

IV. DISCUSSION

Values of the equipartition magnetic field, minimum energy, and the implied synchrotron lifetimes for various regions of the jet and lobes are given in Table 3. A spectral index of 0.6, a lower frequency cutoff of 10 MHz, and an upper frequency cutoff of 20 GHz have been assumed. The energy is relativistic protons has been taken to be zero.

The electron synchrotron lifetimes in the knots are sufficiently long that even modest reacceleration processes in the jet can keep the knots lighted. The lifetimes in the hot spots are much shorter. The hot spot in the NE lobe is apparently now being fed by the jet, so its short synchrotron

TABLE 3

DERIVED PHYSICAL PROPERTIES

Component	Distance from Core (arcsec)	Frequency (GHz)	B_{eq} (μG)	U_{min} (ergs)	τ_{syn} at 5 GHz ($\times 10^6$ yr)
Knot in jet	4	1.4	45	3.1×10^{53}	0.85
Knot in jet	10	1.4	26	1.4×10^{54}	1.8
Knot in jet	30	1.4	18	4.4×10^{54}	3.2
Knot in jet	46	1.4	14	3.3×10^{54}	4.6
Knot in jet	62	1.4	13	5.0×10^{54}	5.3
NE hot spot	121	4.9	97	2.2×10^{55}	0.26
		15.0			0.15
SW hot spot	74	4.9	49	1.4×10^{55}	0.74

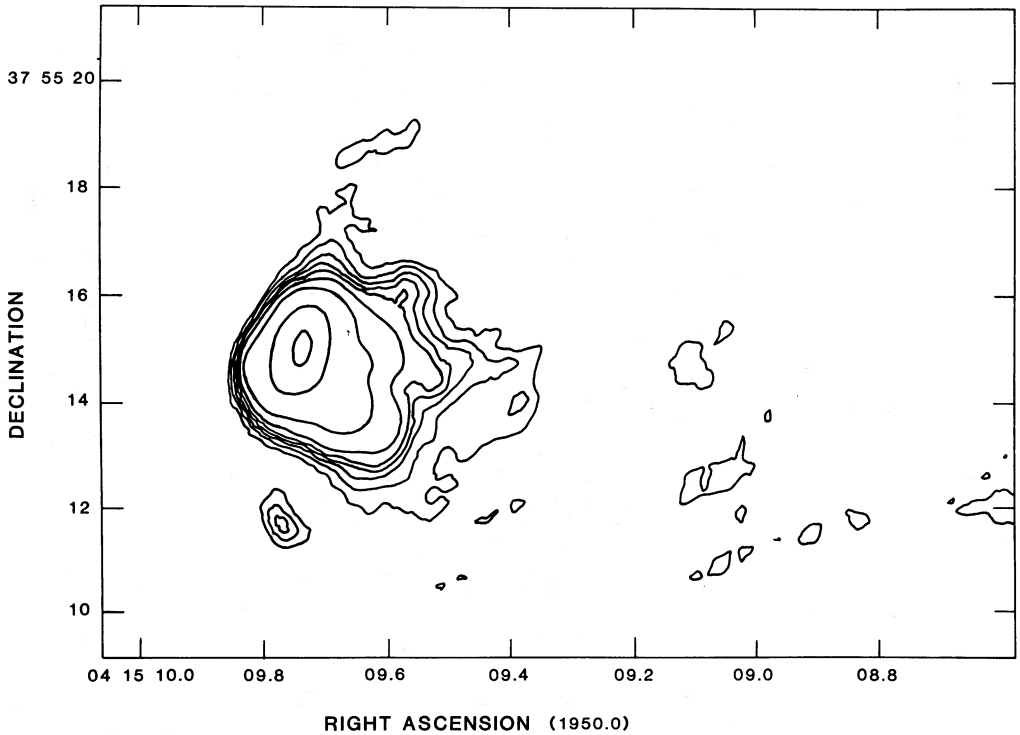

FIG. 7*a*

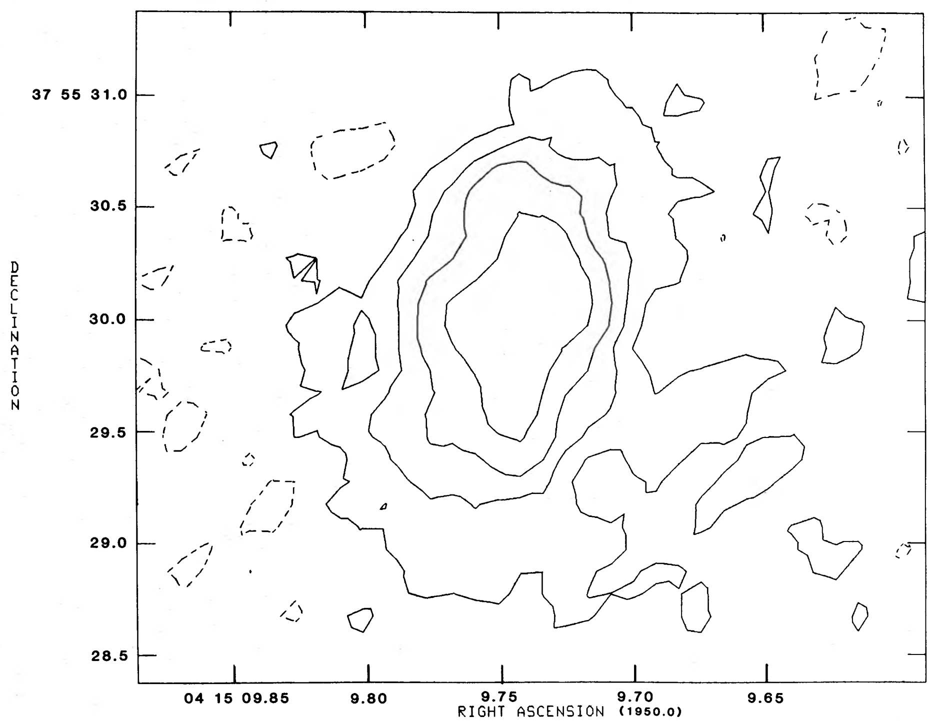

FIG. 7*b*

FIG. 7.—Total intensity maps of the hot spot in the NE lobe. (*a*) At 4.9 GHz, with 0".40 × 0".36 resolution. The contour levels are −1.02, −0.34, 0.34, 0.68, 1.02, 1.36, 1.71, 2.73, 6.1, 27, and 61 mJy per beam. (*b*) At 15.0 GHz, with 0".24 resolution. The contour levels are −0.57, 0.57, 1.7, 2.8, and 4.0 mJy per beam.

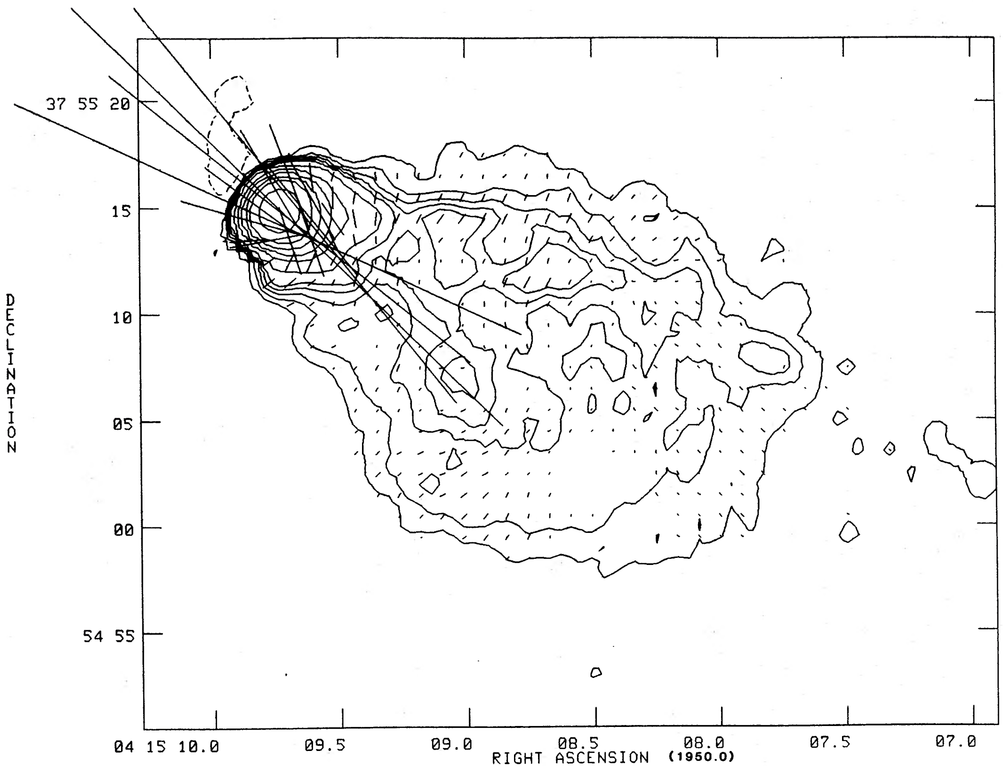

FIG. 8*a*

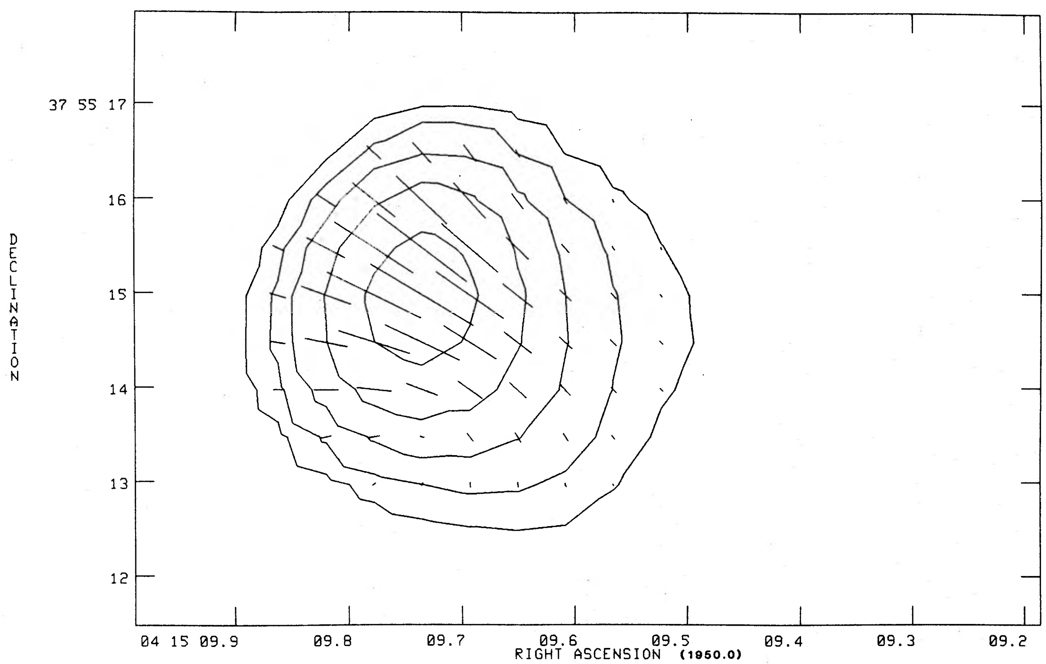

FIG. 8*b*

FIG. 8.—The NE lobe of 3C 111 in linearly polarized emission. (*a*) At 1.4 GHz, with 1".34 × 1".20 resolution. The observed polarization *E*-vectors are plotted; 1" = 0.466 mJy per beam. (*b*) At 4.9 GHz, with 1".31 × 1".24 resolution. The *E*-vector scale is 1 arcsecond = 66.3 mJy per beam.

1984ApJ...279...60L

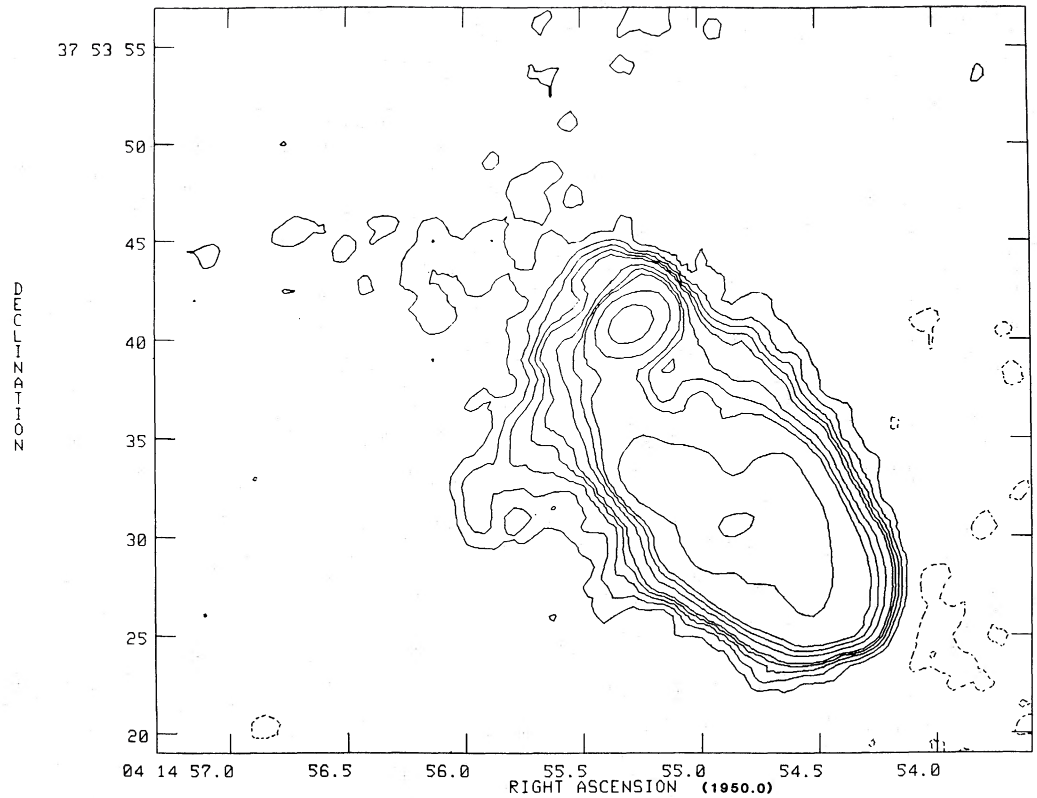

FIG. 9.—Total intensity map of the SW lobe at 1.4 GHz, with 1".34 × 1".20 resolution. Contour levels are −2.3, −0.76, 0.76, 1.51, 2.3, 3.0, 6.0, 8.3, 10.6, 23, and 60 mJy per beam.

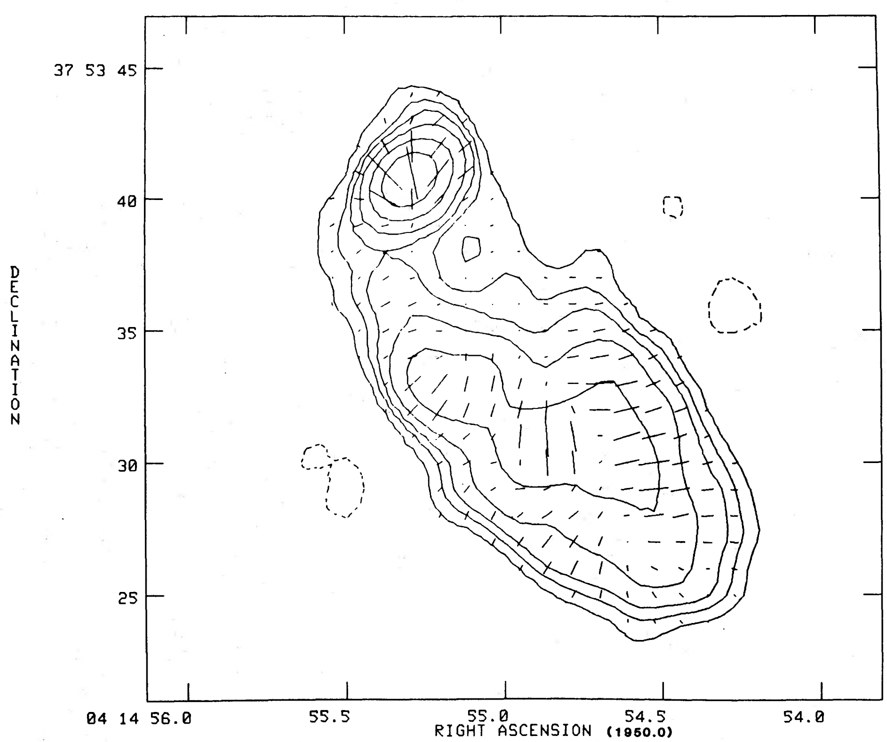

FIG. 10.—The SW lobe of 3C 111 in linearly polarized emission at 4.9 GHz. 1".31 × 1".24 resolution. The E-vector scale is 1 arcsecond = 4.14 mJy per beam.

lifetime (2.6×10^5 yr if $B = B_{eq}$) poses no problem. However, the only slightly longer lifetime in the hot spot in the SW lobe is harder to explain. There is no observed jet, on any scale, to the SW of the core. Either the jet in that direction is currently inactive, or it is active but invisible.

If the first possibility is true (i.e., the observed one-sidedness reflects an intrinsic one-sidedness), then the jet has been one-sided toward the NE for at least $1.2 \times 10^7/v_4$ yr, where $v_4 = v_j/10^4$ km s^{-1}. This conflicts with the synchrotron lifetimes in the SW hot spot unless $(B/B_{eq})^{-1.5} v_4 > 12$.

If there is an active but unobserved jet feeding the SW lobe, there is the problem of explaining why the jet to the NE is visible, while the jet to the SW is not. As mentioned in § III, the jet:counterjet flux ratio is >3:1 on a kiloparsec scale. On a parsec scale the constraint is stronger. Any jet to the SW on that scale is at least 15 times weaker than its counterpart to the NE (Linfield 1981). Differential Doppler boosting of an identical jet:counterjet pair will produce a brightness ratio of $[(1 + \beta_j \cos\theta)/(1 - \beta_j \cos\theta)]^{2+\alpha}$, where θ is the angle between the jet and the line of sight. This requires $\beta_j \cos\theta > 0.46$ on a parsec scale, and $\beta_j \cos\theta > 0.20$ on a kiloparsec scale. VLBI observations provide no constraint on the jet velocity on a parsec scale, but on a kiloparsec scale, several arguments (discussed below) suggest that $v_j \sim 10^4$ km s^{-1}. The uncertainties are large, however, and jet velocities as large as 10^5 km s^{-1} cannot be ruled out. There are no strong constraints on θ, but small values ($<6°$) would imply a large (>2 Mpc) source size.

A more likely cause of the unobserved counterjet is an intrinsic asymmetry. Such an asymmetry is suggested by the angles subtended at the core by the two hot spots (0°.7 for the hot spot in the NE lobe vs. 1°.6 for the hot spot in the SW lobe). If the jet:counterjet radius ratio equals the ratio of these opening angles, this could easily produce a ratio >3 in the flux per unit length. Why the opening angles should differ by a factor of 2.4 for the jet and counterjet is unclear, but this phenomenon is exhibited by 3C 31 (Bridle *et al.* 1980) and NGC 315 (Willis *et al.* 1981).

The SW lobe has a very peculiar shape, with a hot spot at the trailing edge. The contrast in surface brightness between the hot spot and the remainder of the lobe is more prominent on maps with higher resolution than those shown in Figures 9 and 10. The hot spot is nearly aligned with the jet (the hot spot has a PA of $-122°$ with respect to the core, only 2°–3° less than the PA of the reflection of the jet through the core), whereas the remainder of the lobe is much less well aligned (the PA of the lobe center is $-125°$). This suggests that the lobe (exclusive of the hot spot) is a relic from earlier jet activity, with its original hot spot now faded. The currently observed hot spot, at the termination of an active (or recently active) jet, is much younger and is superposed upon the older lobe. The reduced surface brightness in the region just south of the hot spot (Figs. 9 and 10) is consistent with a separate origin for the hot spot. The difference in PA (as seen from the core) of the old lobe and the current hot spot can be explained either as a relative motion between the core and intergalactic medium, or as a rotation of the jet nozzle.

Perley, Bridle, and Willis (1984) discuss several methods of estimating jet velocities. For the jet in 3C 111, these methods give velocities in the range 5000–12,000 km s^{-1}, with considerable uncertainties. Each of these methods depends on jet density and/or acceleration efficiency in the hot spot, both of which are unknown.

a) *Confinement of Jet*

As shown in Figure 5, the jet undergoes significant collimation in the inner 30″; its rate of expansion $d\Omega/d\Theta$ drops by a factor >5. It is almost certainly confined at distances $>30''$ from the core. The velocity in a dissipationless, supersonic, expanding jet will increase with distance, provided that it is confined. A free jet has no such acceleration mechanism; its opening angle will be constant. It is of interest to determine whether or not the jet confinement is due to the thermal pressure of the surrounding gas. Several constraints can be placed on the proposed confining gas cloud, as was done for parsec scale jets by Linfield (1982). The radius of this spherical cloud will be set at 30 kpc, to ascertain whether or not the jet is thermally confined at this distance.

The first constraint is that the pressure of the gas must be sufficient to confine the jet. Synchrotron theory yields a minimum internal pressure for the jet ($P_{min} = 0.53 U_{eq}$/Volume), assuming that its brightness is not strongly Doppler boosted. Adopting the calculated minimum pressure gives

$$n_e T > \frac{P_{min}}{1.95k} \text{ (for 70\% hydrogen by mass)} . \tag{1}$$

This is a conservative limit (e.g., the contribution from relativistic protons has been taken to be zero). A value of $P_{min} = 7.0 \times 10^{-12}$ dyn cm^{-2} has been used (cgs units will be used throughout this discussion). This is a factor of 2 less than the minimum pressure of the knot at 30″, in order to partially compensate for the uneven brightness distribution in the jet.

A second constraint can be imposed from the lack of an observed radio halo around the core. Several processes, including synchrotron emission and Thompson scattering, will contribute to the halo flux. To provide a firm upper limit to the electron density, it will be assumed that Thompson scattering is the only emission process operating (it requires only that the gas be ionized):

$$\tau_{Thomp} < \ln\left(\frac{S_{halo} + S_{core}}{S_{core}}\right) \approx \frac{S_{halo}}{S_{core}} \quad \text{if} \quad \tau_{Thomp} \ll 1 ,$$

where S_{halo} is the flux from the inner 30″ of the halo.

$$n_e < \frac{\tau_{Thomp}}{R\sigma_{Thomp}} . \tag{2}$$

A 1.4 GHz map (4″.5 resolution) made with strongly tapered data gives an upper limit to the flux of a 30″ radius halo of 90 mJy. This yields an upper limit to τ_{Thomp} of 0.09. Therefore, $n_e < 1.6$.

X-ray observations provide a powerful constraint in this source. The X-ray flux is variable; the extended thermal emission must be less than or equal to the lowest flux measured (3.0×10^{-11} ergs cm^{-2} s^{-1} in the 2–10 keV band; Feigelson and Berg 1983). This upper limit gives

$$\epsilon_{ff}(n_e, T) < \frac{L_x}{(4/3)\pi R^3} , \tag{3}$$

where $\epsilon_{ff}(n_e, T)$ is the free-free emissivity per unit volume in the 2–10 keV band, and $R = 30$ kpc. An isothermal sphere with constant pressure has been assumed. This is appropriate for a gas cloud confined by the potential of a cluster. Any nonuniformity in T or n_e will increase L_x for a given average pressure.

Other constraints arise from the need to keep the gas heated. McKee and Cowie (1977) give an analytic approximation to the cooling function. For $10^5 < T < 4 \times 10^7$ K, this equates to a cooling time of $\tau_{\rm cool} = 2.1 \times 10^{-5} n_e^{-1} T^{1.6}$ yr. If the gas cloud is static, it must be heated on a time scale shorter than this. If there is a bulk expansion or contraction, a resupply of hot gas (rather than reheating of existing gas) is also allowed. The static case will be considered first. Free-free absorption of nonthermal radiation from the core is an inadequate heating source, because of the very low optical depth. Mechanical heating is much more efficient. We consider two ways of setting a time scale for this. The first assumes that there is one supernova every 10 years, which inputs 10^{51} ergs into mechanical heating. This is an upper limit to the expected heating from supernovae. In combination with the cooling time, this yields

$$n_e < 4.1 \times 10^{-5} T^{0.3} . \quad (4)$$

An alternative way of deriving a time scale for mechanical heating assumes that the energy source propagates at the sound speed. Requiring the sound speed crossing time from the core to 30 kpc radius to be less than the cooling time gives

$$n_e < 1.0 \times 10^{-16} T^{2.1} . \quad (5)$$

For a static cloud this adds no constraints not already imposed by conditions (1) and (4). However, unlike condition (4), condition (5) applies in the nonstatic case, provided that the outflow or inflow (less likely) is not supersonic.

The constraints imposed by conditions (1)–(5) are plotted in Figure 11. For conditions (4) and (5), the additional constraint that $\tau_{\rm heat} < 3 \times 10^7$ yr is included. Galaxy mergers can potentially heat the gas on time scales $> 10^8$ yr. If $\tau_{\rm heat} = 3 \times 10^7$ yr and $\tau_{\rm heat} < \tau_{\rm cool}$, then $n_e < 7.0 \times 10^{-13} T^{1.6}$. A confining cloud with $T < 10^8$ K is essentially excluded. For $T > 10^8$ K, a large region of parameter space is allowed. However, a 30 kpc gas cloud this hot could not be confined by the galaxy or by the cluster. The alternative is an outflow. An outflow at the sound speed would have a mass flux at 20 kpc of

$$M = 1.6 \times 10^5 T_8^{0.5} n_e M \text{ yr}^{-1} .$$

Typical values of $M > 100 \, M_\odot \text{ yr}^{-1}$ are required, which seems unlikely.

b) *Magnetic Confinement and Stability*

As thermal confinement of the jet appears unlikely, we consider the alternative: magnetic self-confinement. Polarized emission was only detected from the inner 1".5 of the jet; the field configuration in the region where collimation occurs is therefore not known. In the few cases where jets in high-

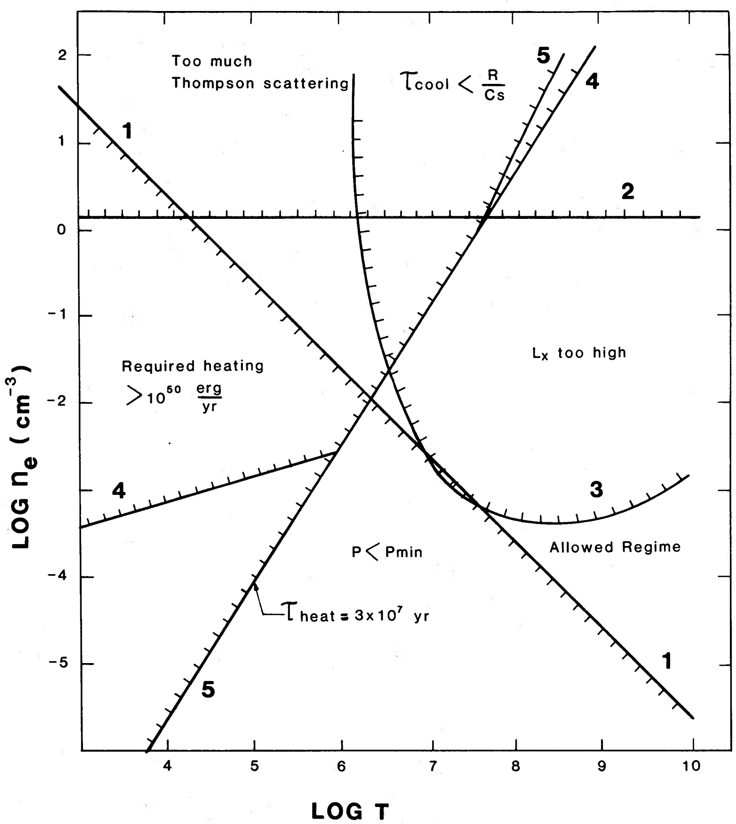

FIG. 11.—Constraints on a possible gas cloud confining the 3C 111 jet. Below line 1, the thermal pressure is less than the calculated minimum synchrotron pressure. Above line 2, the Thompson scattering would be greater than is observed. Above line 3, the X-ray emission would be greater than is observed. Above line 4, a mechanical energy input rate greater than 10^{50} ergs yr^{-1} would be required to keep the cloud heated. Above line 5, the gas would cool more quickly than the sound speed crossing time. For lines 4 and 5, the additional constraint that the heating time is less than 3×10^7 yr has been imposed.

luminosity sources such as 3C 111 have been mapped in polarized intensity, the projected magnetic field is parallel to the jet. Such a configuration would not provide any confinement. Magnetic confinement could result from a longitudinal surface current, producing an azimuthal field outside the observed jet. The effects of the return current would be small if it were distributed throughout a large cross sectional area.

A magnetically confined plasma is subject to a variety of hydromagnetic instabilities (Chandrasekhar, Kaufman, and Watson 1958). An axial magnetic field slows or prevents these instabilities, but the required field strength is not known for the case of a jet surrounded by a fluid of different density. The most likely instabilities to be observable in large-scale jets are long-wavelength pinching ($m = 0$) or helical ($m = 1$) modes, because these instabilities can grow to large amplitudes before the jet is disrupted (Hardee 1982). Also, an axial magnetic field preferentially stabilizes short wavelength instabilities.

The six well-defined knots in the 3C 111 jet (Fig. 2*b*) have a rather regular spacing of $\sim 20r_j$, suggesting the existence of a pinching mode instability. Cohn (1983) has calculated the growth rates of these instabilities for a magnetically confined jet with zero internal field. He found that for Mach number $\mathscr{M} = 4$ (his highest velocity case) the growth rate for $\lambda \sim 20r_j$ is $\sim 0.02c_s/r_j$ (c_s is the sound speed in the jet), and drops roughly linearly with increasing wavelength. For 3C 111, where $\mathscr{M} \sim 10$–20 appears plausible (if the jet is free in the inner 20″), such an instability would thus require a time $> 30\tau_{\rm flow}$ to fully develop. ($\tau_{\rm flow}$ is the length of time for matter to flow the length of the jet.) This instability cannot be the cause of the observed knots unless the "pinches" are convected along the jet at less than $0.03v_j$. If the instability is inhibited by an axial field, as expected, the upper limit to the convection velocity is still lower (Cohn assumed zero axial field).

Norman *et al.* (1982) and Norman, Winkler, and Smarr (1983) have done extensive numerical modeling of jets. They found that high Mach number ($\mathscr{M} > 6$) jets are stable, due to a backflow from the jet termination, which forms a cocoon. In their models of low- and intermediate-luminosity jets, periodic oblique shocks propagate into the jet. Such shocks induce particle acceleration; this is a plausible cause of the knots observed in 3C 111.

c) Variation of Jet Intensity with Θ

There is no detectable emission between the knots for $\Theta > 15''$. The falloff in jet intensity for $\Theta < 15''$ is much slower than expected for an adiabatically expanding jet. However, if strong particle acceleration occurs at knots (as discussed above), additional acceleration between the knots may be unnecessary.

On a sub-arcsecond scale, the jet brightness drops much more rapidly with distance. VLBI observations (Linfield 1981) measured a jet brightness of $3.3 \times 10^4 \Delta_{\rm VLBI}^{-1}$ Jy arcsec^{-2} at 10.7 GHz and $\Theta = 0\farcs004$. (Δ is the ratio of jet width to beamwidth.) The jet brightness at 15.0 GHz; $\Theta = 0\farcs25$ is $< 65\Delta_{\rm VLA}^{-1}$ mJy arcsec^{-2}. If $\alpha = 0.6$, $I_\nu \propto \Theta^{-k}$, then $k > 3.1 + 0.24 \ln(\Delta_{\rm VLA}^{-1}/\Delta_{\rm VLBI}^{-1})$. Model-fitting of the VLBI observations yields an opening angle $\sim 6°$, so that $\Delta_{\rm VLA}$ and $\Delta_{\rm VLBI}$ probably do not differ by more than a factor of 2 or 3. This observed intensity variation is much steeper than that in most arcsecond-scale jets and suggests that the jet may be free in the inner few kiloparsecs, with little or no reacceleration occurring. For adiabatic expansion, $I \propto \Omega^{-5} v_j^{-1.4}$ if B is parallel to the jet, and $I \propto \Omega^{-3.4} v_j^{-3}$ if B is perpendicular to the jet (Perley, Bridle, and Willis 1984). The jet velocity is probably constant or declining with increasing distance, so that either case could apply to 3C 111.

VI. CONCLUSIONS

High-resolution observations of 3C 111 have revealed highly asymmetric structure in a double radio source. The following conclusions are drawn from these observations.

1. The highly collimated jet seen to the NE of the core appears to be strongly supersonic ($\mathscr{M} > 10$). It may be free in the inner 20″ but is confined thereafter.
2. Thermal pressure of the external medium is probably inadequate to confine this jet. Magnetic confinement is suggested, despite the lack of evidence of confining fields.
3. This jet feeds the bright, compact hot spot in the NE lobe. A similar, but broader and fainter hot spot in the SW lobe suggests the existence of an active counterjet. This counterjet is unobserved, perhaps due to its being less well collimated than the observed jet. The cause of this hypothesized weaker collimation is unknown. The peculiar geometry of the SW lobe suggests that the hot spot is superposed upon an older lobe which is not currently being fed.
4. The observed jet has six prominent knots, with separation $\sim 20r_j$ in each case. This type of periodic knot structure is a likely consequence of oblique shocks propagating through the jet, as found in the numerical models of Norman *et al.* (1982) and Norman, Winkler, and Smarr (1983).
5. Comparison with VLBI observations (Linfield 1981) shows a very steep falloff in jet intensity in the inner kiloparsec, consistent with adiabatic expansion.

We thank J. Arons and E. Zweibel for helpful discussions. J. Dreher kindly allowed the use of his 4.9 GHz data in advance of publication. The National Radio Astronomy Observatory is operated by Associated Universities, Inc., under contract with the National Science Foundation. This research was supported in part by NSF grant AST 81-14717.

REFERENCES

Baars, J. W. M., Genzel, R., Pauliny-Toth, I. I. K., and Witzel, A. 1977, *Astr. Ap.*, **61**, 99.
Bridle, A. H., Henrikson, R. N., Chan, K. L., Fomalont, E. B., Willis, A. G., and Perley, R. A. 1980, *Ap. J.* (*Letters*), **241**, L145.
Chandrasekhar, S., Kaufman, A. N., and Watson, K. M. 1958, *Proc. Roy. Soc. London*, A, **245**, 435.
Clark, B. G. 1980, *Astr. Ap.*, **89**, 377.
Cohn, H. 1983, *Ap. J.*, **269**, 500.
Dreher, J. W. 1981, *A.J.*, **86**, 833.
Fanaroff, B. L., and Riley, J. M. 1974, *M.N.R.A.S.*, **167**, 31P.
Feigelson, E. D., and Berg, C. J. 1983, *Ap. J.*, **269**, 402.
Hardee, P. E. 1982, *Ap. J.*, **257**, 509.
Hargrave, P. J., and Ryle, M. 1974, *M.N.R.A.S.*, **166**, 305.
Linfield, R. 1981, *Ap. J.*, **244**, 436.
———. 1982, *Ap. J.*, **254**, 465.
Longair, M. S., Ryle, M., and Scheuer, P. A. G. 1973, *M.N.R.A.S.*, **164**, 243.
McKee, C. F., and Cowie, L. L. 1977, *Ap. J.*, **215**, 213.
Norman, M. L., Smarr, L., Winkler, K.-H. A., and Smith, M. D. 1982, *Astr. Ap.*, **113**, 285.
Norman, M. L., Winkler, K.-H. A., and Smarr, L. 1983, *Astr. Ap.*, submitted.

Perley, R. A., Bridle, A. H., and Willis, A. G. 1984, *Ap. J. Suppl.*, **54**, 291.
Readhead, A. C. S., Cohen, M. H., and Blandford, R. D. 1978, *Nature*, **272**, 131.
Schwab, F. 1980, *Proc. Soc. Photo-Opt. Instr. Eng.*, **231**, 18.
Simard-Normandin, M., Kronberg, P. P., and Button, S. 1981, *Ap. J. Suppl.*, **45**, 97.
Thompson, A. R., Clark, B. G., Wade, C. M., and Napier, P. J. 1980, *Ap. J. Suppl.*, **44**, 151.
Willis, A. G., Strom, R. G., Bridle, A. H., and Fomalont, E. B. 1981, *Astr. Ap.*, **95**, 250.

R. P. Linfield: 264-781, Jet Propulsion Laboratory, 4800 Oak Grove Drive, Pasadena, CA 91103

R. A. Perley: National Radio Astronomy Observatory, P.O. Box 0, Socorro, NM 87801